Applied Mechanics and Materials *Online: 2013-01-25*
ISSN: 1662-7482, Vols. 284-287, pp 727-732
doi:10.4028/www.scientific.net/AMM.284-287.727

Effects of Number of Circumferential Casing Grooves on Stall Flow Characteristics of a Transonic Axial Compressor

Jin-Hyuk Kim[a], Kyung-Hun Cha[b] and Kwang-Yong Kim[c]

Department of Mechanical Engineering,

Inha University 253, Yonghyun-Dong, Nam-Gu, Incheon, Republic of Korea

[a]jinhyuk@inha.edu, [b]kyunghun@inha.edu, [c]kykim@inha.ac.kr

Keywords: Axial compressor, Numerical analysis, Casing treatment, Total pressure ratio, Adiabatic efficiency, Stall margin.

Abstract. This work investigates the effects of circumferential casing grooves on stall flow characteristics of a transonic axial compressor. Numerical analysis is conducted by solving three-dimensional steady Reynolds-averaged Navier-Stokes equations with the shear stress transport turbulence model. The results of flow analysis for an axial compressor with smooth casing are validated in comparison with experimental data for the pressure ratio and adiabatic efficiency. The numerical stall inception point is identified from the last converged point by convergence criteria, and the stall margin is predicted numerically. The peak adiabatic efficiency point is also obtained by reducing the normalized mass flow in the high mass flow region. In order to explore the influence of number of the circumferential casing grooves on the performance of the compressor, the stall margins and peak adiabatic efficiencies are evaluated compared to the case smooth casing. The stability of the axial compressor with circumferential casing grooves is found to be sensitively influenced by the number of grooves.

Introduction

Recently, compressor stability becomes an important issue as a performance parameter as well as pressure ratio and efficiency, and it is limited by stall and surge in low mass flow range [1]. Stall and surge induce a large vibration of the compressor blades resulting in high blade and casing stress levels which are often unacceptable for structural reasons. These flow phenomena in a compressor ultimately result in the instability [2].

Tip leakage vortex and its trajectory, which can be caused by the gap geometry near blade tip region, are generally known as major factors to induce instabilities like stall and surge in an axial compressor. To control this flow phenomenon, the circumferential casing grooves, as one of the casing treatment methods, have been introduced to the design of an axial compressor. And, many studies have been carried out to improve the stability of the compressors with the circumferential casing grooves through experimental and numerical methods.

Wenzel et al. [3] experimentally measured the individual stage characteristics and overall performance of a multi-stage axial compressor with the casing grooves. Bailey [4] evaluated on the effects of the depth, location and number of the casing groove in a single-stage axial compressor through the experimental test. Shabbir and Adamczyk [5] numerically demonstrated the flow mechanism for the stall margin improvement on an axial compressor with application of the grooves. Wu et al. [6] reported numerical and experimental parametric investigations on a high-speed small-scale compressor with the grooved casing treatment. Houghton and Day [7] performed both experimental and computational studies to investigate the effect of axial location of a single casing groove on the stability and efficiency of a subsonic axial compressor. Kim et al. [8] presented the performance evaluation on the stall margin and efficiency of a transonic axial compressor with various circumferential casing grooves.

In this work, the effects of number of the circumferential casing grooves on the stall flow and performance characteristics of an axial compressor have been numerically analyzed based on three-dimensional Reynolds-averaged Navier-Stokes (RANS) equations. The stall margins and peak

adiabatic efficiencies with different number of grooves are evaluated and compared with those of the compressor with smooth casing.

Description of the Compressor and Circumferential Casing Grooves

The transonic axial compressor with NASA Rotor 37 is investigated in this work. The rotor operates at a speed of 17,188 r/min, and has the total pressure ratio of 2.106 and adiabatic efficiency of 88.9% at the design mass flow rate 20.19 kg/s. The tip clearance is 0.356 mm (0.47% span), the choking mass flow is 20.93 kg/s, and the near-stall point is 0.925 of the choke flow. More detailed specifications of the compressor model with NASA Rotor 37 are listed in Table 1 [9].

The reference grooves, i.e., the seven grooves reported by the previous work [8] as shown in Fig. 1, have the rectangular shape with depth of 4.272 mm and are evenly spaced from the leading edge to the trailing one. The width of each groove is 10% tip axial chord with a gap of 5 % tip axial chord. In order to reduce the number of casing grooves, the grooves located near the trailing edge of the blade are removed one by one with the locations and dimensions of the remaining grooves unchanged. And, cases 1~7 correspond to numbers of grids, 1~7, respectively.

Numerical Approach

The flow field in a transonic axial compressor is analyzed by solving three-dimensional RANS equations with the k-ω-based shear stress transport (SST) turbulence model through a finite-volume solver, the commercial code ANSYS-CFX 11.0 [10]. In this work, to benefit from the k-ω-based SST turbulence model, resolution of the boundary layer with more than ten mesh points is employed. In addition, the near-wall grid resolution is adjusted to keep first grids from the wall $y+ \leq 2$ to accurately capture wall shear stress, and also to implement a low Reynolds number SST model [11].

A structured grid system is constructed in the computational domain shown in Fig. 2 with O-type grids near the blade surface and H/J/C/L-type grids in the other regions. In the previous work [12], a grid-dependency test was performed with various numbers of grids. From the result, this work uses

Table 1. Design specifications of the axial compressor.

Designed mass flow rate [kg/s]	20.19
Rotational speed [r/min]	17188.7
Total pressure ratio	2.106
Inlet hub-tip ratio	0.7
Blade aspect ratio	1.19
Tip relative inlet Mach number	1.48
Hub relative inlet Mach number	1.13
Tip solidity	1.29
Number of blades	36

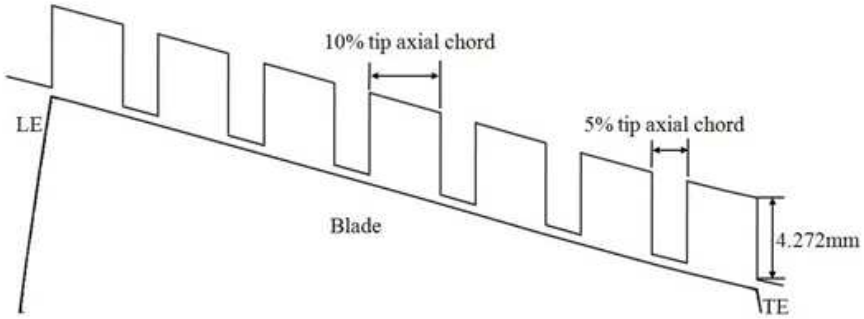

Fig. 1. Schematic diagram of the circumferential casing grooves [8].

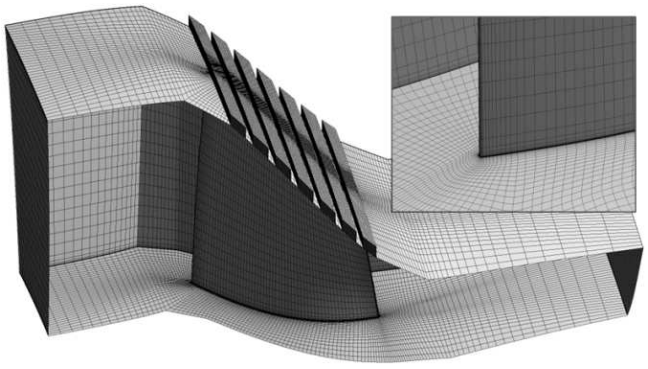

Fig. 2. Structure of the grid system.

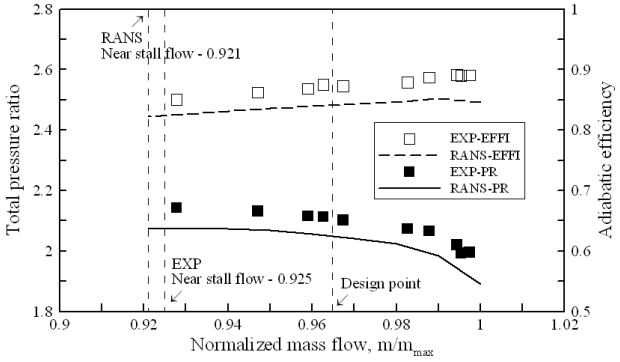

Fig. 3. Validation of the flow analysis [12].

a total of 480,000 nodes to define the main flow passage of the axial compressor. Additionally, each groove is constructed with approximately 24,000 nodes. Fig. 2 shows an example of the grid system used for the axial compressor with the circumferential casing grooves in this work.

The working fluid is considered as an ideal gas in this work. Total pressure and total temperature at the inlet are set to 101,325 Pa and 288.15 K, respectively. The designed mass flow rate for one passage is set at the outlet. The solid surfaces in the computational domain are considered to be hydraulically smooth and adiabatic. The periodic boundary is set at the blade passage interface, and tip clearance is considered along with the passage. The general grid interface (GGI) method is used for the connection between the passage and the circumferential grooves, where the grids on either side of the two connected surfaces do not match [10].

The computations were performed by an Intel Core I7 CPU 2.67GHz PC. And, computational time per single analysis was approximately 6–7 hours.

Validation of Numerical Results

The three-dimensional RANS results have been validated in comparison with experimental data [9] by the previous work [12]. The compressor model used in this test did not employ the casing grooves. Fig. 3 shows the validation results for the performance curves of the total pressure ratio and adiabatic efficiency. The results show some uniform underestimations of the total pressure ratio and the adiabatic efficiency throughout the entire mass flow range, but they are in good agreement with the test results, qualitatively. The numerical stall inception point was identified from the last converged point by reducing the normalized mass flow by 0.002. The peak adiabatic efficiency point is also found by reducing the normalized mass flow by 0.002 in the high mass flow region. This work used the following convergence criteria suggested by Chen et al. [13] to find the numerical stall inception point;

- The inlet mass flow rate variation is less than 0.001 kg/s for 300 steps.
- The difference between the inlet and outlet mass flow rate is less than 0.5%.
- At that time, the adiabatic efficiency variation is less than 0.3% per 100 steps.

In Fig. 3, the near-stall point predicted based on these convergence criteria is 0.921, while the near-stall point measured by the experiment is 0.925, which is the mass flow normalized by choking mass flow. Therefore, it is assured that three-dimensional RANS results based on this convergence criteria are valid and reliable.

Results and Discussion

Performance Characteristics. In this work, the stall margin (SM) and the peak adiabatic efficiency (η) are used as the performance parameters to quantitatively evaluate the compressor stability. These important performance parameters are defined as follow;

$$SM = \left(\frac{m_{peak}}{m_{stall}} \times \frac{PR_{stall}}{PR_{peak}} - 1 \right) \times 100\% \quad (1)$$

$$\eta = \frac{(\frac{P_{t,out}}{P_{t,in}})^{\frac{\gamma-1}{\gamma}} - 1}{(\frac{T_{t,out}}{T_{t,in}}) - 1} \tag{2}$$

where, m and PR indicate the mass flow rate and total pressure ratio, respectively, and the subscripts peak and stall refer to the peak adiabatic efficiency point and the near-stall point, respectively. Also, γ, P_t, and T_t indicate the specific heat ratio, total pressure, and total temperature, respectively.

Fig. 4 shows the performance curves of the total pressure ratio and adiabatic efficiency in case with the smooth casing and cases with different groove numbers. As shown in Fig. 4, it is predicted that the near-stall points are 0.921 for the smooth casing and 0.925, 0.930, 0.915, 0.902, 0.888, 0.891, and 0.882 for cases 1~7 (i.e., number of grooves 1~7), respectively, which are obtained by the aforementioned criteria. The total pressure ratios for the smooth casing and cases 1~7 at the near-stall points are 2.073, 2.069, 2.090, 2.104, 2.099, 2.085, 2.091, and 2.086, respectively. In comparison with the smooth casing, the circumferential casing grooves contribute to a significant reduction of the near-stall mass flow except for case 1, and thus to the enhancement in the stall margin. Higher total pressures are also achieved in most of the range between the peak efficiency and stall points, except for case 1. The peak adiabatic efficiency slightly decreases when the circumferential casing grooves are installed. And, the adiabatic efficiency distributions in all cases except for case 7 are similar to that with the smooth casing.

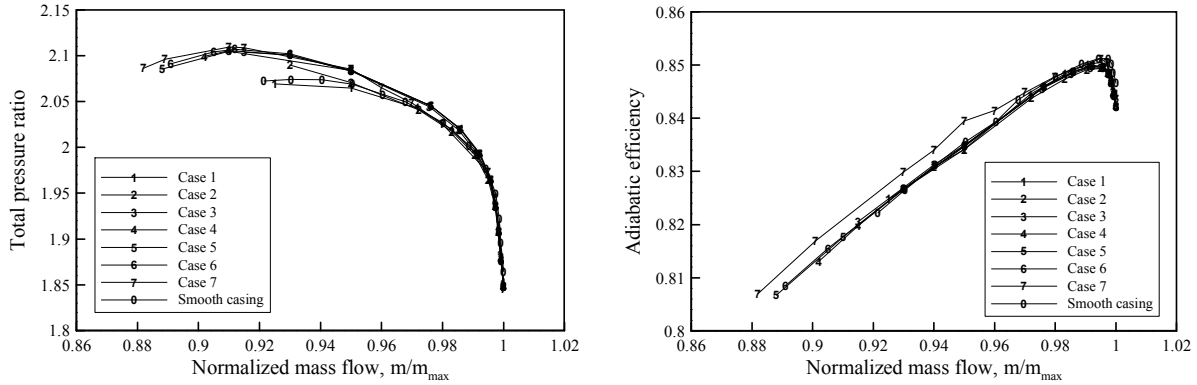

(a) Total pressure ratio (b) Adiabatic efficiency

Fig. 4. Performance curves for the smooth casing and cases with different groove numbers.

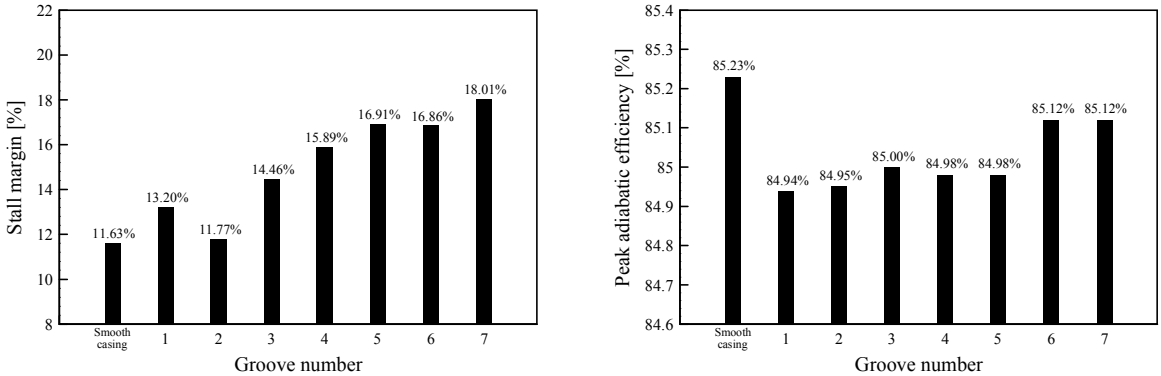

(a) Stall margin (b) Peak adiabatic efficiency

Fig. 5. Comparison of the performance parameters among the cases with smooth casing and different groove numbers.

The stall margin and peak adiabatic efficiency in each case of the circumferential casing grooves are shown in Fig. 5. As shown in Fig. 5(a), all cases of the circumferential casing grooves show a beneficial effect on the stall margin. The stall margin of the smooth casing is 11.63%, and it is increased by the application of the circumferential casing grooves. Case 7 shows the most successful result with the stall margin of 18.01%, which is increased by 6.38% in comparison with the smooth casing. And, the stall margins of cases 1~6 are also increased by 1.57%, 0.14%, 2.83%, 4.26%, 5.28%, and 5.23%, respectively. These results indicate that the cases with smaller groove numbers are less beneficial for the stability. As shown in Fig. 5(b), in all cases with the casing grooves, the peak adiabatic efficiency is decreased compared to the case with smooth casing. The smooth casing shows the highest peak adiabatic efficiency of 85.23%, and the peak adiabatic efficiencies are reduced by 0.29%, 0.28%, 0.23%, 0.25%, 0.25% ,0.11%, and 0.11% for cases 1~7, respectively, in comparison with the smooth casing. Therefore, both the stall margin and peak adiabatic efficiency are generally improved by removing the grooves one by one from the trailing edge. However, some exceptions are found; cases 2 and 6 for stall margin and cases 4-6 for the peak adiabatic efficiency. Especially, the same value for cases 6 and 7 indicates that the last groove does not affect the efficiency but still improves the stall margin.

Internal Flow Characteristics. In order to find the effects of number of the casing grooves on the internal flow characteristics of the axial compressor, cases 2 and 7 have been analyzed and compared with the case with smooth casing. Fig. 6 illustrates the Mach number contours for the case with smooth casing, cases 2 and 7 at the near-stall point of case 2 (normalized mass flow, 0.930). The circumferential casing grooves also affect the momentum transport across the blade tip. As shown in Figs. 6(a) and (c), the separation with the Mach number less than 0.1 is occurred on the suction surface of the blade in the axial compressor with smooth casing, but the separation is suppressed in the axial compressor with circumferential casing grooves and Mach number around the suction surface is eventually recovered in case 7. It is thought that the application of the grooves generates the high momentum flux from the pressure surface to the suction surface. Consequently, the suppressed separation on the suction surface of the blade improves the operating stability.

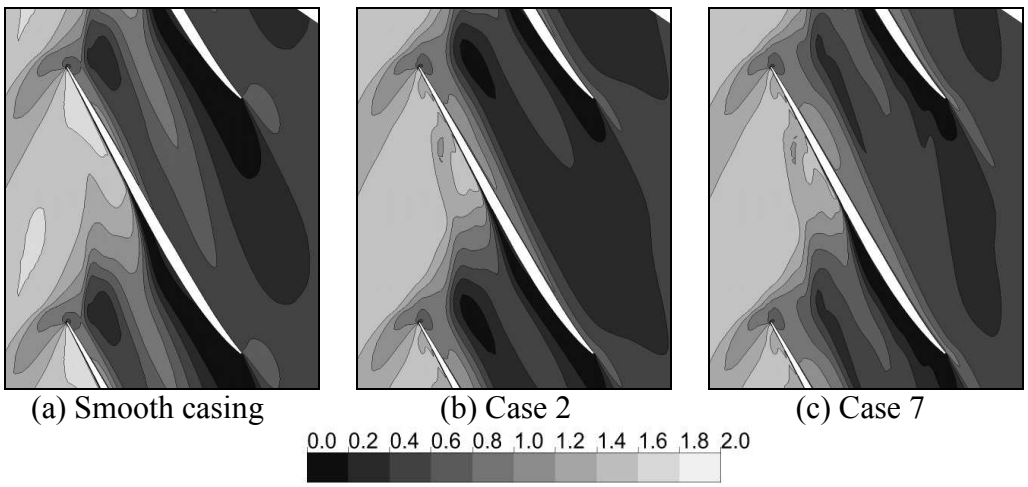

(a) Smooth casing (b) Case 2 (c) Case 7

Fig. 6. Mach number contours at the near-stall point of case 2 (98% span).

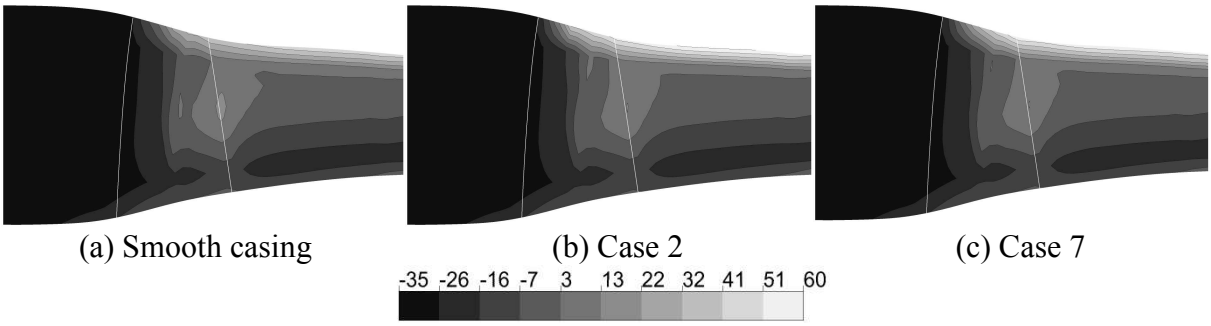

(a) Smooth casing (b) Case 2 (c) Case 7

Fig. 7. Entropy contours on the meridional plane at peak efficiency point [unit: J/kg-K].

Fig. 7 shows the entropy contours for the case with smooth casing, cases 2 and 7 on the meridional plane at each peak efficiency point. The entropy values are area-averaged in circumferential direction. As shown in Fig. 7, the application of the circumferential casing grooves has negative effects in this aspect. Higher entropy generation is observed near the casing of the axial compressor with the circumferential casing grooves; this explains the inevitable decreases in the efficiency of the compressor.

Conclusions

Effects of number of the circumferential casing grooves in an axial compressor on the stall flow characteristics in terms of the stall margin and peak adiabatic efficiency have been numerically analyzed based on three-dimensional RANS analysis. From the results, it is found that application of the circumferential casing grooves is beneficial to reduce the vortex stagnation zone induced by the interaction between the tip leakage vortex and passage shock, and the stability of the axial compressor is influenced sensitively by number of the grooves. And, although there are some exceptions, both the stall margin and peak adiabatic efficiency are generally improved by removing the grooves one by one from the trailing edge. The last groove near the trailing edge of the blade does not affect the efficiency but still improves the stall margin. Therefore, the compressor with seven casing grooves shows the best performance.

Acknowledgments

This work was supported by the National Research Foundation of Korea (NRF) grant funded by the Korea government (MEST) (No. 2011-0015903).

References

[1] H. Tamaki: Int. J Fluid Mach. and Syst. 3, 29 (2010)

[2] E.M. Greitzer: ASME J. Fluids Eng. 102, 132 (1980)

[3] L.M. Wenzel, J.E. Moss, and C.M. Mehalic: NASA Technical Memorandum, National Aeronautics and Space Administration, Washington, D. C. (1975)

[4] E.E. Bailey: NASA Technical Memorandum, National Aeronautics and Space Administration, Washington, D. C. (1972)

[5] A. Shabbir, and J.J. Adamczyk: ASME J. Fluids Eng. 127, 708 (2005)

[6] Y. Wu, W. Chu, H. Zhang, and Q. Li: ASME J. Fluids Eng. 132, 121103 (2011)

[7] T. Houghton, and I. Day: Journal of Turbomachinery Vol. 133, No 2, 021007 (2011)

[8] J.H. Kim, K.J. Choi, and K.Y. Kim, Inst. Mech. Eng., Part A: J. Power and Energy. 226, 218 (2011)

[9] J. Dunham: AGARD Advisory Report 355, (1998)

[10] ANSYS CFX-11.0. ANSYS CFX-Solver Theory Guide, ANSYS Inc. (2006)

[11] F.R. Menter, AIAA J. 32, 1598 (1994)

[12] K.J. Choi, J. H. Kim, and K. Y. Kim: Proceedings of the ASME Turbo Expo 2010, (2010) June 14-18; Glasgow, UK

[13] H. Chen, X. Huang, S. Fu: Proceedings of the 42nd AIAA/ASME/SAE/ASEE Joint Propulsion Conference and Exhibit, AIAA-2006-4799 (2006)